RADIATION NOISE IN A HIGH SENSITIVITY STAR SENSOR

J. B. Parkinson and E. Gordon

Aerojet ElectroSystems Company
Azusa, California 91702

PRA AESC SAMSO 2 March 1971

Abstract

An extremely accurate attitude determination has been developed by Aerojet ElectroSystems Company for space applications. This system uses a high sensitivity star sensor in which the photo multiplier tube is subject to noise generated by space radiations. The space radiation induced noise arises from trapped electrons, solar protons and other ionizing radiations, as well as from dim star background. The individual noise components have been successfully simulated for pre-flight evaluation of the star sensor performance.

The steady trapped electron and the intermittent solar proton environments for a high altitude orbit are related to solar activity. The solar activity and hence the electron and proton environments are predicted through the end of the twentieth century. The available data for the response of the phototube to proton, electron, gamma ray, and bremsstrahlung radiations are reviewed and new experimental data is presented. Prompt and delayed pulses from the faceplate/photocathode and contributions from the dynodes are isolated, and pulse height distributions are given for each.

The predicted electron and proton environments are then combined with phototube response. The average noise due to the relatively steady electron environment is of the order of 10^4 pulses per second compared with 2×10^5 pulses per second for the signal from a single 4.6 magnitude star. For a typical worst solar proton event, the noise will be 10^5 to 10^6 pulses per second, which is comparable to the signal from a nominal 4.6 magnitude star. This noise will typically last about one day. The model for the dim star background averages 3×10^4 pulses per second but varies widely.

A simulation was developed which represents the characteristics of the effect of radiations on the star sensor, including the non-stationarity of the backgrounds.

Introduction

Aerojet ElectroSystems Company has developed a high accuracy attitude determination system for space applications. The system contains a high sensitivity star sensor subject to space radiations. The object of this study is the prediction of the effects of those radiations.

Star Sensor Description

The optical portion of the star sensor collects light from stars and focuses it on the surface of a reticle. When a star image falls on a slit in the reticle, the light from that star can reach the photocathode of an EMR 541E-01 photomultiplier.

The star sensor electronics were designed for photon counting. The counting method eliminates the effects of stochastic variations in anode pulse amplitudes, i.e., there is one count for each cathode photoelectron detected. The circuitry which detects anode pulses outputs a normalized 50 nanosecond pulse for each anode pulse detected. These output pulses are counted throughout a 140 microsecond count cycle. The count value accumulated in each count cycle is transmitted to the ground for processing. The center of the star image requires about 230 microseconds to traverse the slit, so the time at which the center of the image is at the center of a slit can be determined from the count values.

When several photons reach the photocathode simultaneously, their anode pulses overlap, and there is only one normalized pulse for counting purposes. Thus when a high energy electron or proton causes the simultaneous emission of many protons, the star sensor electronics normally outputs only one normalized pulse. However, delayed photon emissions from an incident electron or proton result in several output pulses.

The counts from a star dimmer than seventh magnitude are comparable to the stochastic variations in the total background signal and such stars cannot be detected. The average contribution of stars dimmer than 4.6 magnitude is expected to be 4.2 counts per count cycle although it is much higher in the galactic plane.

Electron and Proton Environments

The trapped electron and solar proton environments are both capable of generating noise in star sensors. Both environments are affected by solar activity.

The detailed relation between solar eruptions and the solar proton and trapped electron environments is very complex, and we are not currently able to predict satisfactorily the specific causitive solar eruptions. However, estimates of the expected electron and proton fluxes can be related to expected smoothed sunspot numbers.

The expected smoothed sunspot numbers are represented by

$$\overline{R} \sim R_o + \Delta R \sin^2 \left[\pi \left(\frac{t}{10.5\,yr} \right)^{3/4} \right] \qquad (1)$$

where

R_o is the expected minimum R (typically 2-10)

ΔR is the expected span of R (typically 50-200)

t is the time from solar minimum (years)

Equation 1 predicts a rise up to 6 months prematurely but is otherwise a good representation of expectancy.

The dates of certain minima and predicted minima (Reference 1) are

Beginning cycle	18	February 1944
	19	April 1954
	20	October 1964
	21	December 1974
	22	September 1985
	23	January 1997

For the parameters in Equation 1,

Cycle No.	R_o	ΔR	Estimated 6-year Mean of R Near Solar Maximum
19	6	195	150
20	8	103	85
Average	5	100	79

Cycle 21 will likely be close to average. Cycles 22 and 23 may be below average, though it is too early to predict with any confidence. For predicting cycles beyond #20, the average values can be used.

For a high altitude orbit, solar proton events may typically occur during the order of 4% a year near solar maximum. Most of the time energetic solar protons will not be encountered. The expected frequency of solar proton events larger than a given ϕ_{max} (proton/cm^2 sec) may be taken as

$$F\left(>E,\ \geq \phi_{max}\right) \sim \frac{700\ \text{proton/cm}^2\,\text{sec}}{\phi_{max}} \left(\frac{\overline{R}}{100}\right)^2 \left(\frac{100\ \text{Mev}}{E}\right)^{3/2} \qquad (2)$$

where

$\overline{R}$ is the smoothed sunspot number

E is proton energy (Mev)

F is the expected number of events per year.

For protons with energies around 50 Mev, solar proton events will generally last from 0.5 to 3 days, with one day being typical. Lower energy protons often arrive later and last for a longer total time. Duration expectancy may be scaled with $\sqrt{E}$. Total proton fluence for all events in a given period of time may be expected to be 2 or 3 times that from the expected single largest event during that period of time.

Equation 2 represents a satisfactory correlation, based on available data from Cycles 19 and 20. However, at energies less than 30 Mev, it tends to overpredict. It also tends to overpredict the number of smaller proton events. Recent data may be conveniently found in the issues of Reference 2.

For the trapped electron environment, the following model will be taken as representative of high altitude equatorial orbits:

$$\phi\left(>E\right) \sim \frac{1 \times 10^7}{\overline{R}/100}\, e^{-\frac{E}{0.21}} + 2 \times 10^6 \left(\frac{\overline{R}}{100}\right)^2 e^{-\frac{E}{0.50}} \ \frac{\text{electron}}{\text{cm}^2\,\text{sec}} \qquad (3)$$

where

R is the smoothed sunspot number

E is electron energy (mev)

A contribution to the electron flux below 0.1 Mev has been neglected.

Equation 3 represents the mean rate averaged over one day. The diurnal extremes are typically a factor of 2 higher at 0830 local time and a factor of 5 lower at 2400 local time.

Primary cosmic ray fluxes will generally range from 4 to 9 particle/cm^2 sec, varying inversely with solar activity. They may be further depressed during solar proton events. The average energy is about 3 Bev.

Photomultiplier Irradiation Results

The phenomenon of ionizing radiation interacting with a vacuum phototube device (e.g., photomultiplier) is believed to occur as follows: (1) a prompt pulse of 1 to several cathode photoelectrons equivalent followed by (2) a train of single photoelectron pulses with the rate of occurrence dying out with time (References 3 and 4). Pulse heights for the prompt pulse and also total pulses per interaction are shown in Table I, as deduced by various investigators for several vacuum phototubes and kinds of ionizing radiation.*

The prompt pulse is believed caused by Cerenkov radiation in the glass faceplate, while the delayed pulse train is thought to be caused by excitations in the faceplate and subsequent decays with emission of optical quanta. Dynode pulses are relatively few in proportion, being less than 0.1% of the total for electrons, bremsstrahlung, and gammas and likely not greater than 0.1% for protons. For very large pulse sizes (above perhaps 20 photoelectrons equivalent) the dynode pulses dominate. However, for photon counting star sensors, the dynode pulses can be neglected.

Aerojet, in cooperation with others, has performed several experiments to measure the pulse height distributions from the photocathode and dynodes of photomultiplier tubes, due to electron, bremsstrahlung, and proton radiations.** To obtain total radiation information, a photomultiplier tube may be used directly. The EMR 541E-01, with trialkali photocathode on 7056 glass (approximately S-20 response) and copper-beryllium venetian blind dynodes, is used in the star sensor. However, to separate photocathode and dynode effects, it was necessary to find a device with large separation of photocathode from the dynodes. An ITT S-412 image dissector tube, trialkali photocathode on 7056 glass (approximately S-20 response) but with silver-magnesium box-and-grid dynodes, provided 4 inches separation and was selected for the supplemental experiments. The effective photocathode area of this tube is approximately 1.8×10^6 times smaller than for the EMR 541 tubes, which further provides excellent isolation of the dynode effects. The faceplate is approximately 35% thicker. The wide separation of the aperture from the photocathode also permits direct determination of the pulse height distribution of delayed pulses without elaborate timing equipment, since prompt photocathode pulses are reduced to single-electron events.

From Sr-90/Y-90 beta and Co-60 and Ra-226 gamma testing of the image dissector, two distinct dynode-region pulse height distributions were evident. Whether the taller of two (Group A) originates from the first dynode or the aperture plate was not determined. The delayed pulse height distribution for the photocathode region was determined from beta tests. Typical spectra for these tests are shown in Figure 1.

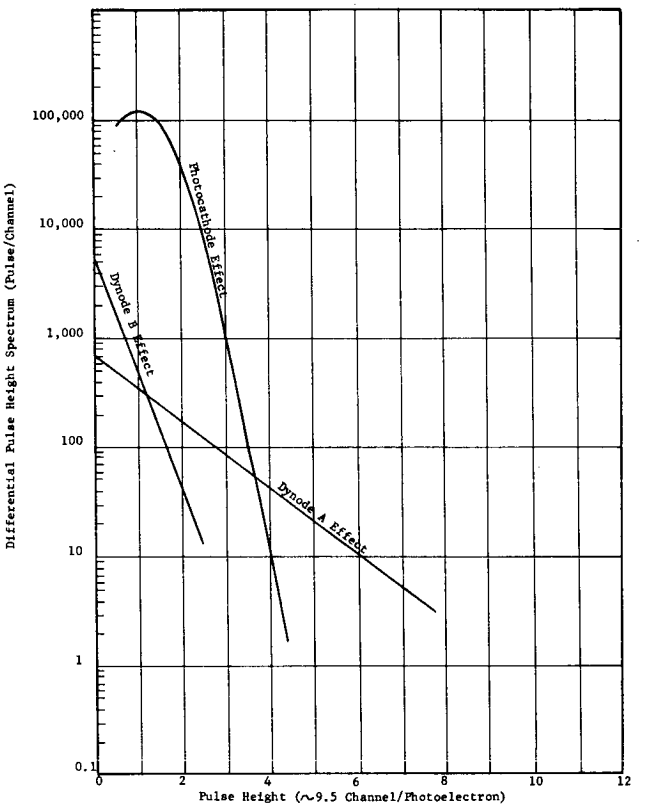

Figure 1
Pulse Height Spectrum Due To A Beta Source (Sr^{90} - Y^{90})

Pulse height distributions from both photocathode and dynode regions were determined for protons at four energies from 22 to 39 Mev. A typical spectrum for these tests is shown in Figure 2. The response to protons is strongly dependent on proton energy, peaking very sharply around 34 Mev.

---

* The luminescence parameter, L, is defined as the photocathode current divided by photocathode area, peak radiant sensitivity, and dose rate.

$$L = \frac{I_c}{S(\lambda_o)\, \dot{D}\, A_c}$$

This luminescence parameter includes the Cerenkov radiation contribution.

** The excellent work and cooperation of Dr. G.F. Knoll, University of Michigan; G. Bain and C.W. Freeborn, ITT; Dr. J. Ryan, MIT Lincoln Laboratory; and L.W. Morton, Aerojet, is hereby gratefully acknowledged. (Miss Freeborn is now at Aerojet.)

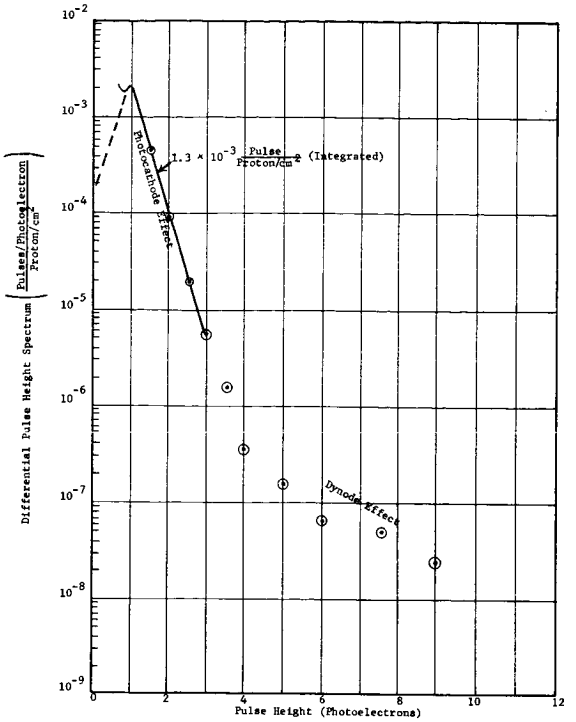

Figure 2
Pulse Height Spectrum Due To A Proton Beam (39 Mev Protons)

The photomultiplier was tested with Sr-90 bremsstrahlung and with bremsstrahlung from electrons at three energies from 0.5 to 3 Mev to determine total pulses above a minimal threshold. The prompt pulse height distribution was not measured. This information has been inferred from data from other investigators and by analogy with the distribution for delayed pulses.

Jerde, Peterson and Stein investigated the pulse height distribution for an RCA 7265 with S-20 response but a very thick soda-lime glass window. Their data for Co-60 indicate about 2.5 to 3 photoelectrons for the large-pulse height distribution, which is to be associated with the prompt pulses. (Their reported value of 10 appears applicable to only a few percent of the pulses in this distribution, and will therefore not concern us further here.) Lacking specific data for the EMR 541E-01, we shall assume the mean prompt pulse size is 3 photoelectrons equivalent. Uncertainties due to difference in faceplate thickness make this estimate somewhere between good and up to a factor of 2 too high.

Dressler and Spitzer offer measurements for the EMR 541E-01 with Co-60 indicating approximately 20% of the total pulses are prompt. Jerde, et al., report for the RCA 7265 about 3%, though their pulse height distribution data appear to indicate a somewhat larger value. Here we shall assume 20% for the EMR 541E-01.

Jerde, et al., for cosmic rays (predominately protons) report 10-20 photoelectrons per prompt pulse. This distribution was observed above 5 photoelectrons pulse size and compares well with 13.8 photoelectrons per dynode pulse observed by AGC/ITT for the image dissector. Comparing with Figure 2, the cosmic ray pulses less than 3 photoelectrons are coming predominately from the photocathode, while those greater than 5 photoelectrons are coming predominately from the dynodes. For large pulses, Cerenkov radiation would, therefore, appear to be a secondary effect with protons even up to cosmic ray energies.

For single-electron counting, Aerojet observed in the image dissector tube approximately 25% fewer pulses/rad with 39 Mev protons than with electrons and gammas. This is just about what would be expected if Cerenkov radiation is absent with protons, but all forms of ionizing radiation are equally effective in producing faceplate excitations. We hereby accept that this is true for photomultiplier tubes as well. Wolff (Reference 8) also finds that photocathode effects of image dissector tubes and photomultipliers are directly scalable with effective area.

Zagorites and Lee (Reference 5) find radiation generated currents are essentially independent of gamma and X-ray energies except around 40-100 kev, where it is probably enhanced by direct interactions with the photocathode or dynodes. Peak enhancement appears to be more than a factor of 3 but not more than an order of magnitude.

The rate of delayed pulses is reported by Dressler and Spitzer to decay in milliseconds. The effective time constant is believed to lengthen out somewhat in time due to the existence of a spectrum of excited states. For most purposes, the early-time time constant will have the greatest impact. In order to have a number to work with tentatively use $\tau = 1 \times 10^{-3}$ sec in the probability equation

$$P = Ae^{-t/\tau}. \qquad (4)$$

For most practical purposes, prompt pulses are instantaneous.

Model for Photomultiplier Radiation Response

A model pulse height distribution for the EMR 541E-01 irradiated by gamma rays, electrons and bremsstrahlung is shown in Figure 3. The models for delayed pulses and dynode pulses are based on experimental data, as described above. The assumed model for prompt pulses is, of course, dependent upon particle energy. For electron energies below about 0.5 Mev, gamma energies below about 0.8 Mev, and bremsstrahlung

generated by electrons with energies below about 1 Mev, the prompt pulses can probably be neglected.

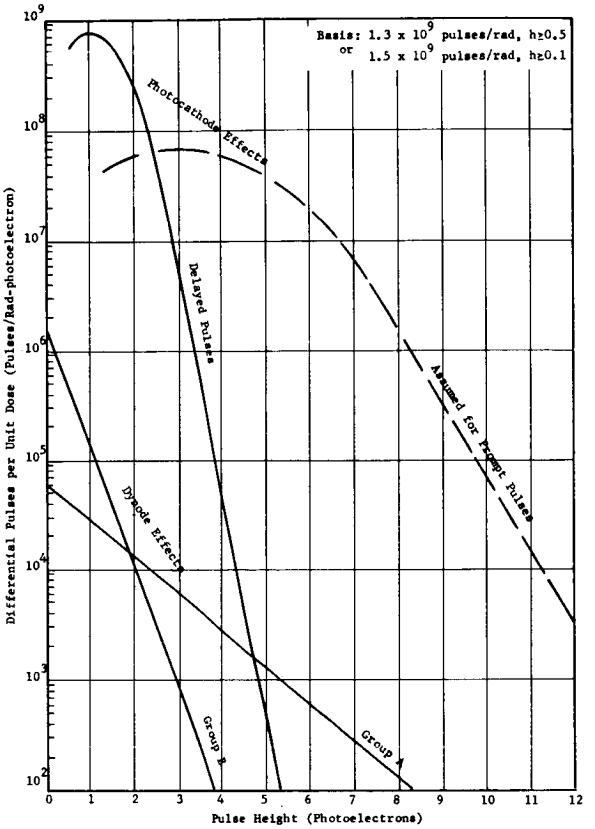

Figure 3
Pulse Height Spectra For An EMR 541E-01 Photomultiplier (Co-60 Gamma Rays)

The pulse height distributions of Figure 3 may be represented analytically:

Photocathode — Delayed Pulses

$$n(h) = 8 \times 10^8 \exp\left(-\left[\frac{h-1}{0.873}\right]^2\right) \text{ pulse/rad-photoelectron, } h < 3$$

$$= 4.2 \times 10^{12} \times 10^{-h/0.5} \text{ pulse/rad-photoelectron, } h \geq 3 \quad (5)$$

Photocathode — Prompt pulses

$$n(h) \sim 0.67 \times 10^8 \exp\left(-\left[\frac{h-3}{2.62}\right]^2\right) \text{ pulse/rad-photoelectron, } h < 9$$

$$\sim 0.35 \times 10^{12} \times 10^{-h/1.5} \text{ pulse/rad-photoelectron, } h \geq 9 \quad (6)$$

Integrated, the delayed pulses are about

1.2×10^9 pulse/rad, $h > 0.1$;

1.0×10^9 pulse/rad, $h > 0.5$;

and the prompt pulses are about

0.3×10^9 pulse/rad, $h > 0.1$ or > 0.5

Dynodes — Group A

$$n(h) = 6 \times 10^4 \exp\left(-\frac{h}{1.3}\right) \text{ pulse/rad-photoelectron} \quad (7)$$

Dynodes — Group B

$$n(h) = 1.5 \times 10^6 \exp\left(-\frac{h}{0.39}\right) \text{ pulse/rad-photoelectron} \quad (8)$$

Integrated, the total pulses are

$$N_A (>h) = 8 \times 10^4 \times 10^{-h/3} \text{ pulse/rad} \quad (9)$$

$$N_B (>h) = 6 \times 10^5 \times 10^{-h/0.9} \text{ pulse/rad} \quad (10)$$

For protons, the analytical representations are:

Photocathode — Delayed Pulses

$$N = 1.1 \times 10^9 \text{ pulse/rad} \quad (11)$$

with distribution above h = 1 given by,

$$N (>h) = 1.3 \times 10^{10} \times 10^{-h/0.75} \text{ pulse/rad} \quad (12)$$

Prompt pulses likely occur only at relativistic proton velocities (i.e., cosmic rays).

Dynode — Group A (32 Mev protons)

$$n_A(h) = 4.4 \times 10^3 \exp\left(-\frac{h}{13.8}\right) \text{ pulse/rad-photoelectron} \quad (13)$$

Dynode — Group B (32 Mev protons)

$$n_B(h) = 8.7 \times 10^4 \exp\left(-\frac{h}{4.6}\right) \text{ pulse/rad-photoelectron} \quad (14)$$

Integrated these become

$$N_A (>h) = 6 \times 10^4 \times 10^{-h/31.8} \text{ pulse/rad} \quad (15)$$

$$N_B (>h) = 4 \times 10^5 \times 10^{-h/10.6} \text{ pulse/rad} \quad (16)$$

Response to proton dose peaks sharply at 32 Mev and is about 4 Mev wide.

Alternatively, the integrated dynode responses may be represented by

$$N_A (\cdot h) = 1.8 \times 10^{-2} \times 10^{-h/31.8} \quad \text{pulse-cm}^2/\text{proton} \tag{17}$$

$$N_B (>h) = 1.35 \times 10^{-1} \times 10^{-h/10.6} \quad \text{pulse-cm}^2/\text{proton} \tag{18}$$

The above representations of dynode pulses are based on data for Ag Mg dynodes. Reed et al. data (Reference 6) indicate CuBe dynodes might be perhaps a factor of 3 less sensitive. Any such differences are overlooked here.

The prompt pulses, including dynode pulses, should be assumed to occur in 10^{-7} seconds or less. The delayed pulse rate probability decays with a time constant of 10^{-3} seconds. For sapphire, Barr and Eberhardt (Reference 9) find the time constant becomes as long as several seconds to half a minute.

Orbital Noise Prediction

The electron environment will be present almost continuously. Therefore, electron-induced noise will also be present almost continuously.

The anticipated electron environment is given by Equation 3. One component is depressed by solar proton activity, while the other is enhanced. At $\bar{R} = 100$, each component will yield about 10^{-6} rad/sec bremsstrahlung at the photomultiplier tube. The primary electrons below 5 Mev will all be stopped in the structure. The worst case for Cycles 20-21 will occur near solar minimum in 1974-1975. If it is assumed $\bar{R} \sim 10$ is representative of 1974, then noise in orbit will be generated by about 1×10^{-5} rad/sec at the photomultiplier tube.

If, from Table I, we accept 0.6 nanowatt (4100A) sec/rad cm^2 for the luminescence of the EMR 541E-01-14 faceplate ($h \geq 0.5$) and 0.07 amp/watt (4100A) peak radiant sensitivity, then the photomultiplier response will be

$$N (>0.5) = 0.6 \times 10^{-9} \frac{\text{watt sec}}{\text{rad cm}^2} \; 5 \text{ cm}^2 \times 0.07 \frac{\text{amp}}{\text{watt}} \frac{1}{1.6 \times 10^{-19}} \frac{\text{pulse}}{\text{amp sec}} \tag{19}$$

$$= 1.3 \times 10^9 \text{ pulse/rad}$$

In this case, virtually all noise generation will be by electron-gamma-delta ray (i.e., Compton electron) interaction. Since only a small percentage of incident electrons will yield delta rays exceeding the approximately 0.5 Mev gammas, the mean prompt pulse height will be only $\bar{h} \sim 1$. Since many interactions will fail to produce Cerenkov radiation, it is possible that Equation 19 overestimates the noise generation by as much as 20%.

Therefore, the predicted mean orbital noise generation is

$$\dot{N} = 1.3 \times 10^9 \frac{\text{pulse}}{\text{rad}} \; 1 \times 10^{-5} \frac{\text{rad}}{\text{sec}} = 1.3 \times 10^4 \text{ pulse/sec} \tag{20}$$

with virtually all pulses averaging $h = 1.0$. The expected number of pulses in one 140 millisecond counting interval is, therefore,

$$\bar{N} = 1.3 \times 10^4 \frac{\text{pulse}}{\text{sec}} \; 140 \times 10^{-6} \text{ sec} = 1.8 \text{ pulse} \tag{21}$$

The high energy solar proton environment will be present only a few percent of the time. Over 90% of the year, solar proton-induced noise should be negligible.

The expected solar proton environment is given by Equation 2. For a typical worst three years $\bar{R} \sim 100$. The star sensor structure, shielding, and surrounding hardware restrict protons reaching the photomultiplier to energies above 50 Mev with an effective acceptance solid angle of about 0.5 hemisphere = 0.25 sphere. For faceplate noise, the maximum solar proton environment from Equation 2 is

$$\phi_{max} \sim 700 \frac{\text{proton}}{\text{cm}^2 \text{ sec}} \left(\frac{100}{100}\right)^2 \left(\frac{100 \text{ Mev}}{50 \text{ Mev}}\right)^{3/2} \text{ per year (3 years)} = 6000 \text{ proton/cm}^2 \text{ sec (>50 Mev, omnidirectional)} \tag{22}$$

Table I

Vacuum Phototube Responses to Ionizing Radiations

Device	Radiation	Luminescence Parameter *	Mean No. of Pulses per Interaction	Prompt Pulse Size (Photoelectrons Equiv.	Investigator & Reference Numbers
Photomultipliers:					
EMR 541E-01	Bremsstrahlung	0.56			AGC
	Co-60	0.61	5		Dressler (3)
	Co-60	0.45			Wey (7)
EMR 541K-05M	Co-60	15	75		Dressler (3)
	Co-60	~38			Wey (7)
	Co-60	~12			Reed (6)
EMR 541A-01	Co-60	0.31	2		Dressler (3)
	Co-60	~0.55			Wey (7)
EMR 541A-05M	Co-60	2.0	~20		Dressler (3)
EMR 541A-05	Co-60	~6.2			Wey (7)
EMR 541A-08	Co-60	1.1	~7		Dressler (3)
EMR 541N-01	Co-60	0.12	~1.5		Dressler (3)
EMR 541N-05M	Co-60	≥2	28		Dressler (3)
EMI 6097S	Co-60, Cs-137 0.035-0.38 Mev X-rays	1.5			Zagorites (5)
Dubkont 6467	Co-60, Cs-137	3.9			Zagorites (5)
RCA 1P21	Co-60, Cs-137	0.6			Zagorites (5)
RCA 7265	Co-60		30	2.5-10	Jerde (4)
	Cosmic Rays	~1	10-30	10-20	Jerde (4)
Image Dissector:					
ITT S-412	Co-60, Ra-226 Sr-90	~1		1.3 (Dynodes)	AGC/ITT
	Protons	~0.7	~10^2	1.25 (Dynodes)	AGC/ITT
				13.8 (Dynodes)	AGC/ITT

* Units of nanowatt (λ max) sec/rad cm^2.

Combining this environment with Equation 11, the faceplate noise will be

$$\dot{N} = 1.1 \times 10^{9} \frac{\text{pulse}}{\text{rad}} \; 6000 \frac{\text{proton}}{\text{cm}^2\text{sec}} \; (0.25)\,(1.5) \times 1.8 \times 10^{-7} \frac{\text{rad cm}^2}{\text{proton}} = 4.4 \times 10^{5} \text{ pulse/sec} \tag{23}$$

where a spectrum correction factor F = 1.5 has been assumed. This rate should endure for about one day.

For the dynode pulses, it can be shown that the effective 32 Mev proton flux reaching the photomultiplier is about

$$\Delta\Phi_{max} \simeq 65 \text{ protons/cm}^2 \text{ sec} \tag{24}$$

Thus, using Equations 17 and 18, the two groups of dynode pulses will be

$$\dot{N}_A = 65 \frac{\text{proton}}{\text{cm}^2 \text{Mev sec}} (4 \text{ Mev}) \times 1.8 \times 10^{-2} \frac{\text{pulse cm}^2}{\text{proton}} \; 10^{-0.5/31.8} = 1.2 \text{ pulse/sec} \tag{25}$$

$$\dot{N}_B = 65 \frac{\text{proton}}{\text{cm}^2 \text{Mev sec}} (4 \text{ Mev}) \times 1.35 \times 10^{-1} \frac{\text{pulse cm}^2}{\text{proton}} \; 10^{-0.5/10.6} = 8 \text{ pulse/sec} \tag{26}$$

The dynode pulses represent only about 0.03% of the total and are, therefore, negligible.

Cosmic rays will generate not more than

$$\dot{N} = 1.5 \times 10^{9} \frac{\text{pulse}}{\text{rad}} \; 9 \frac{\text{particle}}{\text{cm}^2 \text{ sec}} \times 3 \times 10^{-8} \frac{\text{rad cm}^2}{\text{particle}} \simeq 4 \text{ pulse/sec} \tag{27}$$

including prompt pulses of perhaps $h \sim 7$. Cosmic ray pulses also appear to be negligible compared to both the proton-generated and the electron generated noise.

Thus, the maximum expected orbital noise is given by Equation 23,

$$\dot{N} = 4.4 \times 10^{5} \text{ pulse/sec}$$

with virtually all pulses averaging h = 1.0. The expected number of pulses in one 140 microsecond counting interval is therefore

$$\bar{N} = 4.4 \times 10^{5} \frac{\text{pulses}}{\text{sec}} \; 140 \times 10^{6} = 61 \text{ pulses} \tag{28}$$

(For 1971-1973, these figures should be down by a factor of more than four.)

The pulse expectancies will not be entirely uncorrelated. (See Table I for the EMR 541E-01.) After a faceplate interaction, whether producing a prompt pulse or not, the rate probability of delayed pulses at time t afterwards is

$$P(t) = \frac{dN}{dt} = \frac{4}{\tau} \exp(-t/\tau), \tag{29}$$

where τ may tentatively be taken to be 1×10^{-3} sec. Equation 29 applies to both electron- and proton-generated noise. Applied to a 140 microsecond counting interval, the probability of a pulse occuring is

$$P(t) = \frac{4\,(140 \times 10^{-6} \text{ sec})}{1 \times 10^{-3} \text{ sec}} \exp\left(-t/10^{-3} \text{ sec}\right) = 0.56 \exp\left(-t/10^{-3} \text{ sec}\right) \tag{30}$$

From Equations 21 and 28, it may be seen that the expectancy of prompt pulses in a given counting interval is 0.36 and 12.2 for the average electron and expected maximum proton environments respectively. The expectancy of total pulses is 1.8 and 61 respectively.

Star Sensor Simulation

A computer program has been developed to simulate the star sensor performance. The output of the simulation program is used to provide inputs for development and qualification testing of the ground data processing. An earlier version of the simulation was used to evaluate the performance of the Kalman filter used in the attitude determination computations. The output from the star sensor simulation (star count processor) is a sequence of star sensor count values. Since the count cycle duration is 140 microseconds, almost one million of these values must be generated for every two minutes of star sensor operation simulated.

The Star Count Processor is part of a comprehensive simulation program modeling the entire satellite. Another processor in the simulation program is the Slit Crossing Processor which determines the times at which star images cross the center of a slit in the reticle. These

slit crossing times are dependent upon the reticle slit geometry, the satellite dynamics being simulated, and star positions derived from a Star Catalog Data Set containing information from Reference 10. The output from the Slit Crossing Processor is a data set of slit crossing times along with the S. A. O. catalog number of the star and its visual magnitude.

The Star Count Processor is capable of simulating a wide variety of background conditions specified by means of the input parameters discussed below. For example, the parameter EP is used as the Poisson distribution parameter for modelling the arrival of prompt pulses caused by bremsstrahlung from trapped electrons. The parameter, EP, is the expected number of count cycles (140 microsecond intervals) between arrivals of these prompt pulses. Since a Poisson process has exponentially distributed interarrival times (Reference 11), the interval between consecutive prompt pulses due to trapped electrons can be expressed as follows in terms of count cycles,

$$DTNE = -EP \ln (RU) \tag{31}$$

Where RU is a pseudorandom number generated by the computer based upon a distribution uniform on the interval (0, 1). If we let STNE' be the arrival "time" of the preceding prompt pulse due to bremsstrahlung, then the next prompt pulse arrives at

$$STNE = STNE' + DTNE$$

$$= STNE' - EP \ln (RU) \tag{32}$$

A similar logic applies to prompt pulses due to protons, either solar or cosmic, in terms of the input parameter SP, the expected number of count cycles between prompt proton-induced pulses. Hence

$$STNP = STNP' - SP \ln (RU) \tag{33}$$

As noted previously, the delayed pulses following a prompt pulse have a rate of occurrence dying out with time. This characteristic is modeled by means of the decay factors, DE and DP, for electrons and protons respectively. Then defining

RE = expected number of output pulses in any count cycle due to electrons

RP = expected number of output pulses in any count cycle due to protons

EN = an input parameter related to effect of each trapped electron

PN = an input parameter related to effect of each solar proton

Then attaching a prime to designate values of RE and RP from the preceding count cycle, we have

$$RE = (RE' + n_e \, EN) \, DE \tag{34}$$

$$RP = (RP' + n_p \, PN) \, DP \tag{35}$$

where

n_e = number of prompt pulses due to trapped electrons in the preceding count cycle

n_p = number of prompt pulses due to solar protons in the preceding count cycle

When the processing for the current count cycle begins, its index, SNC, is obtained by adding one to the previous value of the index. If the previously generated value of STNE is less than or equal to the new value of SNC, then EN is added to RE'. A new value of DTNE is generated if STNE $\leq$ SNC based on a new random number RU. The value of DTNE is then added to the current value of STNE. The process is repeated until the new value of STNE exceeds the current value for SNC. Similar logic is used for STNP with PN being added to RP.

The star background effects vary as the star sensor optical axis sweeps across the celestial sphere. Let b_o be twice the number of radians swept in 1020 count cycles and K be the number of blocks of 1020 count values which have been generated so far in this simulation. The expression

$$XS = \frac{.25}{1.25 + \sin b_o \, K} \tag{36}$$

has a maximum value of 1.0 when the sine function is -1 and a minimum value of 1/9 when the sine function is $+1$. Then the expected contribution from stars dimmer than seventh magnitude is

$$BD = BDI * XS \tag{37}$$

where

BDI = an input parameter equal to the expected contribution of stars dimmer than seventh magnitude in the galactic plane.

Contributions of stars brighter than seventh magnitude must be represented on an individual basis. Although stars dimmer than 4.6 magnitude could have been represented on the same basis as the brighter stars, it was

found that the extra computational cost was not justified. Instead, the following simplified representation was used. These intermediate intensity stars were simulated in terms of an exponential distribution of interarrival times using the quantity SD as the expected interarrival parameter and

$$SD = SDI / (0.15 + XS) \quad (38)$$

where

SDI = an input parameter 1.15 times the expected interarrival time in count cycles in the galactic plane.

The quantity SD is used in the same manner as the parameters EP and SP resulting in the equation

$$STND = STND' - SD \ln(RU) + 3 \quad (39)$$

The three is added to avoid overlap of these stars.

The intensity of the simulated star is given by

$$QD = QM / (.1 + RU) \quad (40)$$

where QM = input parameter nominally equal to one-tenth the response of the star sensor to a 4.6 magnitude star.

The timing of the slit crossing with respect to the count cycles is given in terms of another random number, Z, as follows

$$RD1 = (ZH - Z)QD \quad (41)$$

$$RD2 = QD \quad (42)$$

$$RD3 = (Z + ZH - 1.0)QD \quad (43)$$

where ZH = an input parameter equal to the half width of the slit in count cycles.

If either of the parenthetic expressions is negative, then that value of RD is set equal to zero and the deficiency is removed from RD2. With ZH equal to .82, the expression (ZH - Z) would be negative for any value of Z greater than .82. Physically, this corresponds to the situation in which the slit crossing occurs so late in the second count cycle of the set of three containing the star signal that none of the signal occurs in the first count cycle and there is a short delay before the signal starts in the second count cycle.

Conclusions

1. Vacuum phototubes are good dosimeters for both high energy electrons and bremsstrahlung radiations. This characteristic is essential to predicting sensor response to space radiation.

2. Vacuum phototube response to protons is sensitively dependent upon proton energy.

3. In the single-electron counting mode, virtually all photomultiplier pulses originate in the faceplate/photocathode. This becomes important in design shielding.

4. Star sensor response to the radiation environment of space may be readily simulated with an appropriate computer program.

REFERENCES

1. Bell, Barbara and Wolbach, John G, "Lunar Eclipses and the Forecasting of Solar Minima," Icarus 4, pp. 409-414 (1965).

2. Solar Geophysical Data, Comprehensive Reports; monthly, NOAA.

3. Dressler, K. and Spitzer, L., Jr., "Photomultiplier Tube Pulses Induced by Gamma Rays," Rev. Sci. Instr. 38, pp. 436-438 (1967).

4. Jerde, R. L., Peterson, L. E., and Stein, W., "Effects of High Energy Radiations on Noise Pulses from Photomultiplier Tubes," Rev. Sci. Instr. 38, pp. 1387-1394 (1967).

5. Zagorites, H. A. and Lee, D. Y., "Gamma and X-ray Effects in Multiplier Phototubes," IEEE Trans Nucl. Sci. NS 14, 6, pp. 190-194 (1967).

6. Reed, Edith I., Bowler, Walter B., Aitken, Charles W. and Brun, Jean Francis, "Some Effects of Mev Electrons on the OGOII (POGO) Airglow Photometers," GSFC, NASA X-613-67-132 (March 1967).

7. Wey, W. and Schrier, Joel, Hughes Aircraft Company, Private Communication.

8. Wolff, C., "The Effect of the Earth's Radiation Belts on an Optical System," Appl. Optics 5, pp. 1838-1842 (1966).

9. Barr, F. H. and Eberhardt, E. H., Final Report, "Research and Development of an Improved Multiplier Phototube," ITT/IL -Fort Wayne, Nov. 16, 1966. N67-27365, Contract NASw 1038.

10. Smithsonian Astrophysical Observatory Star Catalog, Washington: Smithsonian Inst. (1966).

11. Parzen, E., Modern Probability Theory and Its Applications, p. 262, New York: John Wiley & Sons (1960).